Thin Films of Poly(*N*-isopropylacrylamide) End-Capped with *n*-Butyltrithiocarbonate

W. Wang,[†] K. Troll,[†] G. Kaune,[†] E. Metwalli,[†] M. Ruderer,[†] K. Skrabania,[‡] A. Laschewsky,[‡] S. V. Roth,[§] C. M. Papadakis,[†] and P. Müller-Buschbaum*,[†]

Physik-Department LS E13, TU München, James-Franck-Str. 1, 85747 Garching, Germany; Inst. Chemie, Potsdam Universität, Karl-Liebknecht-Str. 24-25, 14476 Potsdam-Golm, Germany; and HASYLAB at DESY, Notkestr. 85, 22603 Hamburg, Germany

Received December 13, 2007; Revised Manuscript Received February 13, 2008

ABSTRACT: Thin thermoresponsive hydrogel films of poly(*N*-isopropylacrylamide) end-capped with *n*-butyltrithiocarbonate (nbc-PNIPAM) are prepared on solid supports having silicon oxide surfaces with spin-coating. The film thickness is varied from 5 to 240 nm. As measured with optical microscopy, atomic force microscopy, and X-ray reflectivity, the films are homogeneous and smooth for films thicker than 5 nm. Microbeam grazing-incidence small-angle X-ray scattering (μGISAXS) shows that these nbc-PNIPAM films are physically cross-linked gels, where the end-group domains form the physical cross-links with a defined nearest-neighbor distance of 25 nm. Along the surface normal, with μGISAXS the presence of long-ranged correlations between substrate and film surface is detected. The thinner the nbc-PNIPAM films are, the stronger is the response to swelling in saturated water vapor atmosphere. A swelling up to a factor of 6.5 as compared to the dry film and a factor of 2.9 as compared to the collapsed film is found. The transition temperature in thin films shifts slightly as compared to the bulk, and the width of the transition is film thickness dependent. Measurements of the bulk solution behavior complete the investigation.

1. Introduction

Responsive hydrogels are water-based cross-linked polymer networks that can be designed to expand and contract in response to various external stimuli such as temperature, pH, liquid composition, and electric stimulation.[1,2] Thermoresponsive aqueous polymer systems are known to exhibit large, reversible conformational changes in response to small thermal stimuli.[3] Thermosensitive polymer materials, often called intelligent, can be used as actuators,[4,5] artificial muscles,[6,7] solute separators,[8,9] drug delivery systems,[10–13] thermoresponsive surfaces,[14–16] light modulation systems,[17,18] optical switching devices,[19] and molecular recognition agents.[20,21]

Depending on the type of cross-links, physical and chemical gels are distinguished. Physical gels are held together by polymer chain entanglement and/or by attractive forces present between the network polymers, whereas in chemical gels the polymers are covalently cross-linked.[22]

Poly(*N*-isopropylacrylamide) (PNIPAM) is probably among the most studied thermosensitive polymers.[23–33] PNIPAM in water exhibits a phase transition at a lower critical solution temperature (LCST), which has been investigated by a variety of experimental techniques in the dilute and concentrated regimes. The LCST of PNIPAM in water is approximately at 32 °C and thus slightly less than body temperature, which makes PNIPAM a representative of environmental-sensitive polymers studied for biomedical applications.[34] The temperature-driven change in the conformation of single PNIPAM chains and the macroscopic phase separation reflect rather subtle changes in polymer/water interactions, primarily the release of water molecules from a polymer hydration layer into bulk water. Several models have been described to account for the coil-to-globule collapse of PNIPAM in water and the complex water/PNIPAM phase diagram.[35–37] At low temperatures, intermolecular hydrogen bonds between water and polar groups of PNIPAM solubilize the polymer. Above the LCST the hydrogen bonds break, and hydrophobic associations between the collapsed polymer chains take place.

Slight changes in the chemical composition of PNIPAM have important consequences on the water/PNIPAM phase diagram. The LCST of PNIPAM can be raised or lowered via introduction of hydrophilic or hydrophobic comonomers, respectively.[38] Moreover, the phase transition temperature depends not only on the level of hydrophobe incorporation and on its chemical structure but also on its position on the chain.[39,40] With decreasing molecular weight the effect of end groups of PNIPAM homopolymers increases.[41] In general, the introduction of hydrophobic end groups affects the phase behavior of PNIPAM solutions 2-fold: The miscibility of the polymer in water becomes poorer as a result of direct interactions between water and the hydrophobic end groups. In addition, the mixing entropy of the polymer chains is reduced due to the increase of their apparent molecular weight via micelle formation. Both factors favor phase separation, and the LCST tends to decrease.[42]

In water, polymers which carry a hydrophobic group at one chain end tend to form core−shell structures in which the hydrophobic core is insulated from the water by a brushlike corona of PNIPAM chains.[43,44] PNIPAM carrying a hydrophobic group at each chain end form another type of micelle in water-based solution. The micelles are described as flowerlike associates consisting of loops of hydrated polymer chains having both end groups entrapped in the micellar core.[45] Compared to the large body of work on water-based PNIPAM solutions, thin PNIPAM films are less frequently investigated. This is surprising as many advanced applications of responsive hydrogels are based on thin films and make use of the switching of the film properties at LCST. For example, below the LCST a PNIPAM-coated surface shows a hydrophilic behavior; however, when heated above the LCST, the behavior changes to hydrophobic.[46] This effect on substrates offers the ability to control important interfacial phenomena such as wetting,[47,48] fluid flows,[49] adhesion,[50] and the reversible adsorption of biomolecules as a

* Corresponding author: Ph +49 89 289 12451, Fax +49 89 28912473, e-mail muellerb@ph.tum.de.
[†] TU München.
[‡] Potsdam Universität.
[§] HASYLAB at DESY.

10.1021/ma7027775 CCC: $40.75 © 2008 American Chemical Society
Published on Web 04/15/2008

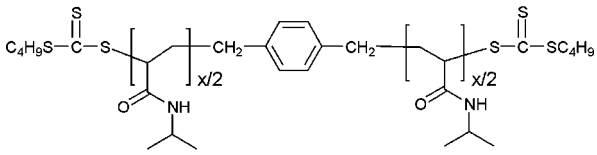

Figure 1. Chemical structure of nbc-PNIPAM ($x = 172$).

function of temperature.[51] Thus, having thermoresponsive surfaces, which undergo a strong change in wetting and adhesive properties triggered by a change in temperature, are much desired. So far, several different techniques were reported for the preparation of thin PNIPAM films: micelle and vesicle adsorption from solution,[52] plasma polymerization,[53] solution casting,[54] layer-by-layer deposition,[55,56] self-assembled monolayers,[57] spin-coating,[58,59] dip-coating,[60] and surface graft polymerization.[61–70] Grafting PNIPAM to surfaces is a promising strategy for creating responsive surfaces, since the physical properties of PNIPAM are readily controlled by changing the temperature. Spin-coating appears to be an interesting alternative, being on the one hand widely used in many areas of thin polymer film preparation and being on the other hand well suited to control film thickness over a broad range.

In the case of triblock copolymers with two polystyrene (PS) blocks sandwiching a central PNIPAM block all well-known microphase separation structures were reported.[59] Depending on the ratio between PS and PNIPAM, the ABA-type copolymers self-assemble into spherical, cylindrical, lamellar, or double-gyroid morphologies. Swelling of the middle block leads to physically cross-linked gels, where the end-block domains form the physical cross-links. In the triblock copolymer terminology the investigated end-capped homopolymer investigated in this work can only allow for the spherical morphology due to the chosen short hydrophobic chain ends.

Because pure PNIPAM homopolymer films miss the possibility of internal cross-links to build up a gel, the addition of hydrophobic chain ends (a triblock copolymer in the extreme case) is a simple way to overcome this problem. However, with increasing glassy, hydrophobic block length the ability to swell decreases. In case of the triblock copolymer P(S-*b*-NIPAM-*b*-S) bulk compositions with spherical PS domains and a PNIPAM continuous phase swell very well in water, whereas composition resulting in cylindrical PS domains or in the bicontinous gyroid structure in bulk swell only by a factor of 3 to 5, respectively. Finally, lamellar compositions do not show any swelling. Along this line short hydrophobically end-capped PNIPAM chains might be expected to exhibit the strongest swelling, thereby maintaining the gel character.

Within the present work we apply the spin-coating technique, which is widely used in many polymer systems but only rarely applied to PNIPAM, for the preparation of thin films. Instead of a PNIPAM homopolymer, we focus on hydrophobically end-capped PNIPAM to address the question if end-capped PNIPAM in thin films undergoes microphase separation and creates an internal structure. At each chain end a very short hydrophobic end group, *n*-butyltrithiocarbonate, was chosen (denoted nbc-PNIPAM, see Figure 1). Reversible addition−fragmentation chain transfer (RAFT) polymerization, being an extremely versatile, controlled free radical polymerization technique for the synthesis of well-defined polymer architectures, was applied to obtain nbc-PNIPAM, using a bifunctional bis(trithiocarbonate) as chain transfer agent.

The nbc-PNIPAM can be considered as the limiting case of a triblock copolymer with a middle PNIPAM block and extremely short hydrophobic end blocks. In solution the association of telechelic polymers into micelles and networks leads to an effective molecular weight higher than that of the

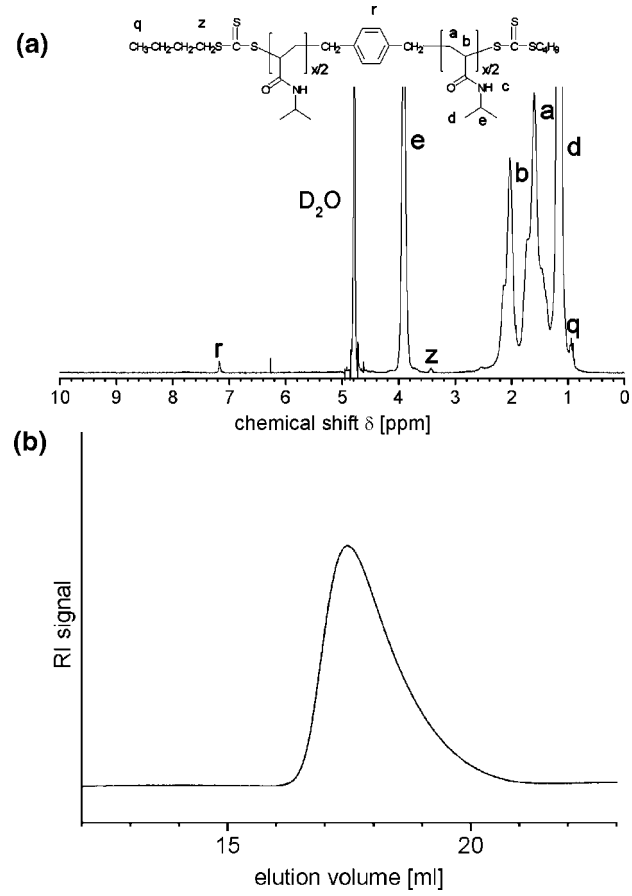

Figure 2. (a) ^{1}H NMR spectrum of nbc-PNIPAM ($x = 172$) showing the end groups. (b) SEC trace.

corresponding PNIPAM homopolymer, which yields a depression of LCST. Moreover, the mixing entropy of telechelic polymers is lower than that of the homopolymer, and they tend to demix. For thin films the authors are not aware of any investigation focusing on end-group-induced microphase separation. The interaction with the substrate might change the behavior as compared to the bulk.

The structural investigation is based on microbeam grazing-incidence small-angle X-ray scattering (μGISAXS) and is accompanied by optical methods and atomic force microscopy. Thus, the surface and the inner film structure can be accessed. The LCST for the thin nbc-PNIPAM films is probed in swelling experiments in a saturated water vapor atmosphere. It is compared to the LCST of nbc-PNIPAM bulk samples as probed with microcalorimetry and photon correlation spectroscopy.

This article has the following structure: The introduction is followed by an experimental section describing the sample preparation and the experimental techniques applied. The next sections show results and discussion on the bulk investigation of nbc-PNIPAM and the thin film experiments.

2. Experimental Section

Materials. *N*-Isopropylacrylamide (98%, Acros) was recrystallized twice from hexane/benzene (1:1, v/v); 2,2′-azobis(2-methylpropionitrile) (AIBN) (98%, Acros) was recrystallized from methanol. Tetrahydrofuran (THF, Merck, extra pure) was distilled from Na/K. Solvents for UV−vis analysis were spectrophotometric grade, while solvents for synthesis and purification were analytical grade. The CTA 1,4-bis(*n*-butylsulfanylthiocarbonylsulfanylmethyl)benzene was synthesized according to a reported procedure.[71]

The UV band of the thiocarbonyl groups has an absorbance maximum at $\lambda = 309$ nm ($\varepsilon = 33\,600$ L mol^{-1} cm^{-1}) in methanol. This value is used for end-group determination.

Table 1. Molecular Characteristics of nbc-PNIPAM

polymer	theory[a] $M_n \times 10^{-3}$ [g mol^{-1}]	NMR[b] $M_n \times 10^{-3}$ [g mol^{-1}]	UV[c] $M_n \times 10^{-3}$ [g mol^{-1}]
nbc-PNIPAM	34	42.5	39

[a] Calculated as: conversion × [monomer]/[CTA]. [b] Calculated by end-group analysis using the proton signal of the phenylene fragment of the R group in ^{1}H NMR ($\delta = 7.18$ ppm). [c] Calculated by end-group analysis of the UV band ($\lambda = 309$ nm, $\epsilon_{CTA} = 33\,600$ L mol^{-1} cm^{-1} in methanol) of the Z group.

Methods for Polymer Characterization. ^{1}H NMR spectra were taken with a Bruker Avance 300 (300 MHz) spectrometer in D_2O, $CDCl_3$, and d_6-acetone solution. UV−vis spectra were recorded on a spectrophotometer Cary 5000 (Varian). Quartz cuvettes (Suprasil, Hellma, Germany) with an optical path length of 10 mm were used. Size-exclusion chromatography (SEC) of the polymer was run in *N*,*N*-dimethylacetamide containing 0.1% LiBr as eluent at a column temperature of 45 °C, with a setup consisting of an Agilent 1200 isocratic pump, an Agilent 1200 refractive index detector, and two GRAM columns (10 μm, 8 × 300 mm, pore sizes 100 and 1000; PSS GmbH, Mainz, Germany). The SEC setup was calibrated using low-polydispersity polystyrene standards (PSS GmbH, Mainz, Germany).

^{1}H NMR and UV−vis spectroscopy were used to obtain independent information about M_n. For NMR measurements, the concentration of end groups is determined by comparing the intensity of the respective proton signals with those of the constitutional repeat units. Assuming that the amount of initiator-derived polymer chains is negligible, number-averaged molar masses are obtained.

Synthesis of *n*-Butyltrithiocarbonate End-Capped Poly(*N*-isopropylacrylamide). The conditions for the synthesis of *n*-butyltrithiocarbonate end-capped poly(*N*-isopropylacrylamide) polymers, denoted nbc-PNIPAM, were as follows: *N*-isopropylacrylamide (20.0 g, 177 mmol), AIBN (5.8 mg, 3.53×10^{-5} mmol), and the bifunctional CTA (154 mg, 3.54×10^{-4} mol) were dissolved in THF (80 g), and the solution was transferred to a 250 mL round-bottom flask equipped with a magnetic stirring bar and a rubber septum. The solution was deoxygenated by bubbling with N_2 for 1 h, then immersed into a preheated oil bath, and polymerized under stirring for 4.5 h at 65 °C. The polymerization was stopped by cooling the flask quickly by a dry ice/isopropanol mixture. The reaction mixture was diluted with acetone and precipitated into 500 mL of *n*-hexane. After collecting the polymer by vacuum filtration, it was further purified by dialysis against deionized water (dialysis membranes ZelluTrans from Roth, Germany; nominal molar mass cutoff 3500 Da). The aqueous polymer solutions were filtered and lyophilized to obtain the dry polymer as a light yellow powder (11.9 g, 59.5%).

Because the molar mass characterization of PNIPAM and of end-capped PNIPAM is difficult with standard methods due to the strong tendency of the polymer molecules to aggregate or to adsorb on surfaces, several different techniques are applied. The theoretically calculated molecular weight is compared with numbers calculated from an end-group analysis with NMR and UV (see Table 1). In the end-group analysis both R and Z groups were functionalized.[71]

The theoretically calculated molar mass value is lower than the experimentally determined ones. This discrepancy is attributed to the material losses during the purification of the polymers by dialysis. As the calculations are based on the assumption that the isolated yields reflect the true monomer conversions, the theoretically calculated values must be taken as lower estimates only.

Microcalorimetry. Polymer solutions were measured using a VP-DSC microcalorimeter from Microcal LLC (USA) with deionized water as the reference. The microcalorimeter and the reference sample were equilibrated before the measurement. A concentration of 0.25 mg/mL of nbc-PNIPAM was investigated with a scan rate of 0.5 °C/min covering a temperature range from 25 to 44 °C. The measured baseline from water was subtracted. Data were analyzed by use of the software supplied by the manufacturer. The phase-transition temperature (T_{MC}) was taken as the one corresponding to the maximum specific heat capacity (C_p) during the transition.

Photon Correlation Spectroscopy. The dynamic light scattering spectrometer with goniometer and monomode fiber detection (ALV-Laser GmbH, Langen) is equipped with two lasers: a 22 mW HeNe laser at 632 nm (JDS Mod. 1145P) and a 150 mW frequency-doubled Nd:YAG laser at 532 nm (Coherent DPSS 532-150). The correlation function of the scattered intensity was calculated using an ALV-5000/E correlator on a logarithmic time scale ranging from 10 ns to 10 s. For photon correlation spectroscopy (PCS) experiments, the polymer solutions were prepared by dissolving the polymer in deionized water (0.25 mg/mL) or dioxane (5 mg/mL). The solutions were filtered directly into the previously dedusted scattering cells. Data were collected at 90° scattering angle. At each temperature 5−10 measurements of 1 min duration were carried out, and after each temperature change the waiting time was 20 min.

The correlation functions were analyzed by numerical inverse Laplace transformation using the REPES program included in the GENDIST software package.[72] PCS measures the intensity autocorrelation function

$$g_2(\tau) = \langle I(t)I(t+\tau)\rangle / \langle I^2(t)\rangle \quad (1)$$

where τ is the decay time and the brackets represent the ensemble average. The $g_2(t)$ can be related to the field autocorrelation function $g_1(t)$ through the Siegert relation. Using the Stokes−Einstein relation together with the measured refractive index of the solutions, the distribution of hydrodynamic radii $A(R_H)$ is calculated and presented in the equal-area representation, $R_hA(R_h)$ vs $\log(R_h)$. The average hydrodynamic radii R_H were determined from the centers of gravity of the peaks in these distribution functions of hydrodynamic radii.

Substrate Cleaning and Thin Film Preparation. Silicon with an oxide layer surface and glass were used as substrate materials. For cleaning the precut silicon (Si 100, n-type, Silchem) and glass pieces were placed in dichloromethane in an ultrasonic bath for 5 min and rinsed with Millipore water shortly after. Afterward, the substrates were kept for 2 h in an oxidation bath at 75 °C consisting of 1400 mL Millipore water, 120 mL of H_2O_2, and 120 mL of NH_3 to clean the surface from organic traces. Thereafter, the samples were stored in Millipore water. Directly before spin-coating the substrates were rinsed with Millipore water at least five times to remove possible traces of the oxidation bath. The substrates were dried using compressed nitrogen before coating the SiOx surface. Because of this protocol at the Si and glass surface a hydrophilic oxide layer of 5 nm is present, which has a small surface roughness below 1 nm.[73]

Dry hydrogel films were prepared by spin-coating (2000 rpm, 30 s) from 1,4-dioxane at room temperature (relative humidity 50%) onto precleaned silicon substrates. The concentration of the nbc-PNIPAM in 1,4-dioxane was varied from 0.3 to 30 mg/mL to achieve different film thickness. The solutions used for spin-coating were transparent and do not show any sign of aggregates. Several identical samples were prepared to prove the reproducibility.

Optical Microscopy and Atomic Force Microscopy. The sample surfaces were observed with optical microscopy using a Zeiss Axiotech 25H optical microscope with magnifications between 4× and 100×. A Hitachi KP-D50 CCD camera recorded the micrographs.

Using a PARK Autoprobe CP atomic force microscope, the sample surface was probed. All measurements were performed in air at room temperature. The amplitude of the oscillation of the tip was calibrated with respect to the vertical position of the piezoelectric scanner. The distance calibration of the piezocontroller was performed with a standard gold grating. Each scanned micrograph consists of 265 lines, scanned with 0.25 Hz up to 1.0 Hz. Several images were measured for each sample. Micrographs were recorded at different sample positions. Contact avoidance to the sample minimized the tip induced sample degradation. The silicon gold-coated conical cantilevers had resonant frequencies at about $f =$ 60 kHz and a spring constant of ~2.1 N m^{-1}. At each individual

sample position, scans with different ranges from 0.5 μm × 0.5 μm up to 5 μm × 5 μm were performed. From the raw data, the background due to the scanner tube movement was fully subtracted to determine the values of the rms roughness over the complete scan area.

X-ray Reflectivity and Optical Interference Measurements. X-ray reflectivity curves were measured with a laboratory Siemens D5000 diffractometer with a reflectivity extension. A knife edge was mounted above the sample surface to reduce background and control the footprint of the X-ray beam on the sample. The reflectivity measurements were performed at a wavelength of λ = 0.154 nm (secondary graphite monochromator, Cu Kα). Measurements were performed in air with a scintillation counter. A large range of the scattering vector component perpendicular to the sample surface $q_z = 2\pi(\sin \alpha_i + \sin \alpha_f)/\lambda$ was covered to allow for the detection of thickness and surface roughness of the thin films. The fits to the reflectivity data were always performed with a model assuming a native oxide layer and a PNIPAM layer on top. Fitting was performed with the program Parratt3 (version 1.5.2).[74]

Thickness and optical constants (n and k) were measured with the Filmetrics F20 thin-film measurement system (Filmetrics Inc., San Diego, CA). The spot size of the light beam is adjustable from 500 μm to 1 cm. The characteristic intensity oscillations in the reflectance spectrum are analyzed in a wavelength regime from 340 to 1100 nm.

Microbeam Grazing Incidence Small-Angle X-ray Scattering (μGISAXS) Measurements. GISAXS measurements were carried out at the beamline BW4 of the DORIS III storage ring at HASYLAB (DESY, Hamburg).[75] The selected wavelength was λ = 0.138 nm. The beam divergence in and out of the plane of reflection was set by two entrance cross-slits. To operate a microbeam the X-ray beam was moderately focused to the size of (H × B) 40 × 80 μm^2 by using an assembly of refractive beryllium lenses.[76] The sample was placed horizontally on a goniometer. A beam stop was used to block the direct beam in front of the detector (MARCCD; 2048 × 2048 pixels). A second, pointlike movable beam stop was also used to block the specular peak on the detector. The incident angle was set to $\alpha_i = 0.465°$, which is well above the critical angles of PNIPAM (0.148°) and of Si (0.20°). As a result, specular and Yoneda peaks are well separated on the detector, and both the sample surface and the film are probed.[77–80] At the chosen sample−detector distance of 2.09 m the Yoneda and the specular peaks are well separated on the detector, and additional features in the intensity originating from resonant diffuse scattering can be detected for the regime of film thicknesses of the nbc-NIPAM films.[81,82] Because of the simple shape of the two-dimensional GISAXS pattern, structural information is obtained from vertical and horizontal cuts of the 2d intensity distribution.[80]

The vertical cut at $q_y = 0$, called detector cut, contains the information on the structure perpendicular to the surface. Horizontal cuts at constant q_z allow extracting the information (geometry, size distribution, and spatial correlation) of lateral structures. The intensity of the q_y cuts was integrated over a small slice Δq_z in the vertical direction to obtain an improved statistics. In the literature these horizontal cuts are also named GISAXS cuts and out-of plane cuts.[80]

3. Results and Discussion of the Bulk Investigation on nbc-PNIPAM Solutions

The hydrophobically end-functionalized PNIPAM was made by RAFT polymerization using a bifunctional RAFT agent. Whereas the SEC trace indicates a monomodal molar mass distribution, the calibration against polystyrene standard can provide only apparent molar mass values (M_n = 20 kDa, apparent polydispersity index 1.5). Absolute values are obtained by end-group determination by ^{1}H NMR and UV spectroscopy, which use the R and Z end groups, respectively. Using the intensity of the proton signal of the phenylene fragment of the R group in ^{1}H NMR (δ = 7.18 ppm) in comparison to the methin proton on the amide moiety of the polymer, end-group analysis gives a number-average molar mass M_n = 42.5 kDa. End-group analysis via the UV band of the Z group at 309 nm gives M_n = 39 kDa. Both methods provide the same values within experimental precision, thus indicating a very high degree of end-group functionalization. As the end-group determination by UV spectroscopy is a priori more sensitive, the corresponding value of 39 kDa is taken as molar mass of the sample in the following discussions.

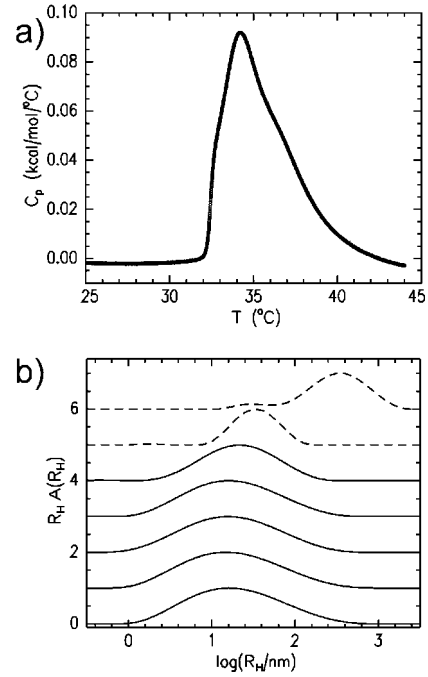

Figure 3. Investigation of aqueous nbc-PNIPAM solutions: (a) temperature dependence of specific heat capacity (C_p); (b) representative distribution functions of hydrodynamic radii R_H probed at different temperatures (from bottom to top: 22, 26, 27, 28, 29, 30, and 31 °C). Curves below the transition temperature T_{PCS} are plotted with solid lines and at or above the T_{PCS} with dashed lines. The curves are shifted along the y-axis for clarity.

For comparison with the structures obtained in the prepared thin hydrogel films, bulk solutions are probed with microcalorimetry (MC) and photon correlation spectroscopy (PCS). Figure 3a shows the temperature dependence of specific heat capacity (C_p) of the PNIPAM aqueous solution in one heating cycle, where the heating rate was 0.5 °C/min. The transition temperature (T_{MC}) is at 34.2 °C. The peak ranges from 32 to 42 °C.

In previous work a systematic shift of the value of T_{MC} toward higher temperatures with increasing molecular weight of the PNIPAM chain was reported in case of hydrophobically end-functionalized PNIPAM.[42] Together with the observation that the magnitude of the molecular weight dependence decreases when using more hydrophobic end groups,[83] our determined value appears to match with both findings because it is higher than the LCST temperature of 32 °C for PNIPAM of similar molar mass but with hydrophilic end groups but lower than the value found for a PNIPAM modified with n-octadecyl chain ends.

With photon correlation spectroscopy (PCS) the hydrodynamic radii of the nbc-PNIPAM molecules or micelles in water are determined. Figure 3b shows representative distribution functions detected at different temperatures. The observed temperature-dependent changes were reversible. Because of the close to log−normal type of distribution function frequently observed in polymeric systems, the curves are shown on a logarithmic x-axis, and the centers of gravity are slightly larger than the maxima of $R_H A(R_H)$. Starting at a temperature of 22

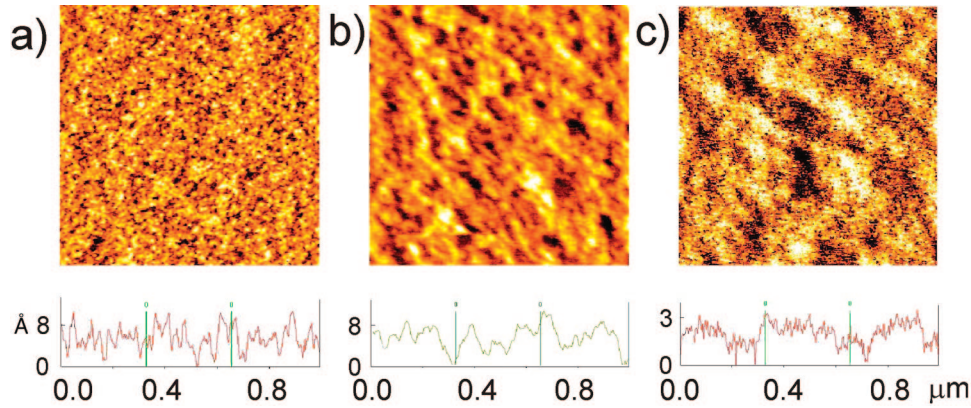

Figure 4. AFM micrographs show a scan size of 1 μm × 1 μm to emphasize on local surface structures for film thickness of (a) 10, (b) 46, and (c) 240 nm. The structure heights increase with the increase in brightness of structures in the images. In the representative line cuts from the AFM data the *x*-axis (lateral, micrometer) differs strongly from the *y*-axis (height, nanometer).

°C the maximum in $R_H A(R_H)$ corresponds to a radius of 16 nm, whereas the average value is $R_H = 36$ nm. For the molecular weight of the investigated nbc-PINPAM an end-to-end distance of 12.4 nm can be estimated. Thus, the measured R_H values suggest the presence of micelles instead of single molecules. For different PNIPAM systems which carry a hydrophobic group at each chain end, a formation of flowerlike associates consisting of loops of hydrated polymer chains having both end groups entrapped in the micellar core was suggested.[42,84] Within the experimental error these micelles remain unchanged up to 28 °C. At 29 °C the shape of the curve $R_H A(R_H)$ changes toward a smaller polydispersity of the micelles, going along with a slight shift of the maximum to 20 nm. At 29 °C, the shape changes; however, the hydration state of PNIPAM remains unchanged.

In solutions heated above 30 °C, an additional peak at higher R_H values appears, and the solution becomes turbid. We assign these findings to the aggregation of several collapsed micelles via interaction of dehydrated PNIPAM chains; i.e., bound water molecules are dissociated into the bulk, and large clusters are formed. The transition temperature $T_{PCS} = 30$ °C determined with PCS is lower than the one probed with MC. This difference between T_{MC} and T_{PCS} is in contrast to the usual behavior observed for PNIPAM solutions, which shows no deviation between the maximum of the thermogram and the onset of turbidity.[85] PNIPAM homopolymer solutions exhibit an LCST of about 32 °C which is attributed to alterations in the hydrogen-bonding interactions of the amide group.[86–89] In cross-linked PNIPAM hydrogels, its LCST temperature in water was found to be 33.2 °C upon heating.[90] However, this transition temperature can be tuned by copolymerizing hydrophobic or hydrophilic comonomers. In case of hydrophobically modified PNIPAM with two *n*-octadecyl chains (C18) end groups the cloud point temperature T_{PCS} detected by light scattering differs significantly from T_{MC}.[42]

End-chain association does not affect the coil-to-globule transition to the same extent as the cloud point because release of the bound water molecules upon heating takes place independently of association, in the ideal limit. Thus, even in the case of the investigated short end groups, the phase separation observed at T_{PCS} is induced by interactions of the hydrophobic termini. The depression in T_{PCS} results from the association of hydrophobically terminated polymers into micelles and networks, which leads to an effective molecular weight higher than that of the corresponding PNIPAM homopolymer. Thus, the mixing entropy of hydrophobically terminated polymers is lower than the one of the homopolymer, and they tend to demix.

In dioxane the scattered intensity is smaller than in water, and moreover, the monoexponential fit to the correlation curve is not describing the data well, presumably because of a certain polydispersity of the diffusing particles. The determined hydrodynamic radius from a REPES analysis is 7.8 nm and thus significantly reduced as compared to water. The reduced polarity of dioxane in comparison with water results in a weaker swelling of the NIPAM segments. Because the interaction is still more favorable between dioxane and NIPAM than between dioxane and the end groups, the presence of micelles with end groups located inside and NIPAM segments outside is still likely. However, instead of the flowerlike associates the shell is more irregular.

4. Results and Discussion of Thin nbc-PNIPAM Films

4.1. Structural Investigation. *a. Dry Hydrogel Film Surface Structures.* Thin nbc-PNIPAM films are prepared with spin-coating from a 1,4-dioxane solution. Compared to other solvents, e.g. water, dioxane turned out to be best suited to achieve smooth and homogeneous films in combination with the described substrate cleaning protocol. The concentration of the solution used for spin-coating is varied from 0.3 to 30 mg/mL to obtain a large range of different film thickness. The spin-coating parameters (spinning speed, acceleration, and spinning time) are kept fixed. Films are prepared at room temperature and thus from solutions containing nbc-PNIPAM micelles with the hydrophobic chain ends located in the micellar core. No aggregates were present in these solutions.

The resulting dry films do not show large scale heterogeneities. With optical microscopy the surfaces appear smooth and continuous, whereas it was reported that very thick and bulk-like PNIPAM gel film (thicknesses on the order of 60 μm) were inhomogeneous on a micrometer scale.[91]

With atomic force microscopy (AFM) the absence of large-scale heterogeneities is confirmed, and the surface topography is visualized with high resolution. Figure 4 shows the example of topography data on a scan size of 1 μm × 1 μm to emphasize on local surface structures for dry film thickness of 10, 46, and 240 nm. All films have a surface structure on the nanometer scale, which is caused by the micelle structure of the nbc-PNIPAM. For 10 nm film thickness (Figure 4a) the presence of the micelles as building blocks for the hydrogel film is best seen. With increasing film thickness the surface structures coarsen laterally but decrease in height (peak-to-valley amplitude) from 0.8 to 0.3 nm. At larger film thickness the attractive surface interaction is weaker for the topmost nbc-PNIPAM micelles, and a larger number of micelles are stacked which allows for an improved space filling with polydisperse spherical soft objects.

b. Density Profile of Dry Hydrogel Films. The density profile along the surface normal is determined with X-ray reflectivity

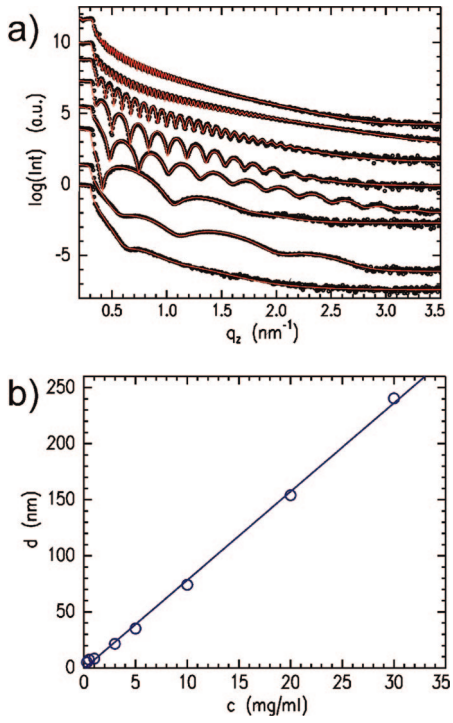

Figure 5. (a) Representative X-ray reflectivity data (dots) shown together with model fits (lines) for the thickness regime covered in this investigation. With increasing film thickness (5, 7, 8, 22, 35, 74, 154, and 241 nm from bottom to top) the curves are shifted along the *y*-axis for presentation. (b) Film thickness *d* plotted as a function of the nbc-PNIPAM concentration of the dioxane solution used for spin-coating. The solid line is a linear fit.

measurements. Figure 5a shows the corresponding data for a selection of the dry nbc-PNIPAM films. From the bottom to the top, the film thickness increases from 5 to 241 nm. Despite in case of the thinnest film, all reflectivity curves exhibit well-pronounced fringes, which extend to large values of the scattering vector component q_z, confirming the homogeneity and small surface roughness. For the thinnest nbc-PNIPAM film the fringes in the reflectivity curve are strongly damped due to the imperfections of the hydrogel layer. Instead of a continuous layer, the SiOx surface is covered with polymer patches. This incomplete surface coverage causes a large surface roughness (peak-to-valley amplitude equal to film thickness). The reason is the micelle structure of nbc-PNIPAM in solution and the limited compressibility of the micelles on the SiOx surface. Because of the applied base surface treatment, the substrate has a hydrophilic oxide surface with a water contact angle of 0° (water can spread on the surface).[92]

Theoretically, a depletion of segments from the surface is present for a neutral or repulsive segment−surface interaction, and an excess of segments is present for an attractive interaction. The magnitude of the excess is dependent upon the strength of the attraction. With neutron reflectivity it was shown that a bilayer profile of end-tethered PNIPAM chains is present in D_2O. It indicates that the attraction of the NIPAM segments to the substrate surfaces is very strong, and a high volume fraction of NIPAM segments in the surface layer forms.[63] Thus, the interaction of the SiOx surface is more favorable for the NIPAM segments. In contrast, the second interface, namely the polymer film surface, is in contact with air (room temperature and relative humidity of 50%). This interface is much less hydrophilic and might even favor the interaction with the hydrophobic *n*-butyltrithiocarbonate end groups. As a consequence, the nbc-PNIPAM micelles are collapsed perpendicular to the substrate surface, and the total height (film thickness of 5 nm) gives the extension along the surface normal. The part of the micelle, which is attracted to the surface via the hydrophobic core, modifies the shape of the micelle from the core−shell structure in solution toward a fried-egg-type structure. A similar behavior was observed with amphiphilic block copolymers adsorbed from solution onto solid substrates.[93,94] Because it is energetically unfavorable to compress the micelles stronger, which would be necessary to make a space-filling homogeneous dry hydrogel film, at a solution concentration of 0.3 mg/mL no more a continuous film is obtained. For the given energetic conditions (hydrophilic SiOx surface) 5 nm is correspondingly the lowest film thickness, which can be prepared from the investigated molecular weight. All films with larger thickness are homogeneous as probed with AFM and X-ray reflectivity.

Unfortunately, the spin-coating process is very complicated and even in the case of simple homopolymers not fully understood. Despite its frequent use in practice, in theory it can only be modeled within a three-step model[95] including many simplifications. The first step describes the early stages, which may have no influence on the resulting structures. In the second step fluid flow reduces the amount of solvent on the rotating sample until in the third step a resulting structure is frozen in due to solvent evaporation. Thus, in the second and third step the concentration of nbc-PNIPAM is increased, which results in the change of the structure. The bridging of micelles in addition to entanglements at high concentrations favors the gelation in hydrophobically end-capped systems, resulting in physically cross-linked hydrogels. Such physically cross-linked thin hydrogel films are extremely desirable because the ability to swell and to react to temperature changes is supposed to be superior to chemically cross-linked systems.

In Figure 5b the linear dependence of the resulting dry film thickness on the concentration used for the spin-coating is shown. Thus, although of micellar type, the simple spin-coating relation still holds and the spin-coating works as with simple polymer solutions (without micelles).[96,97]

Thus, a simple way to control the film thickness for applications of the physically cross-linked thin nbc-PNIPAM hydrogel films is at hand by the concentration of the nbc-PNIPAM solution.

c. Long-Ranged Correlations between Interfaces. Whereas with X-ray reflectivity only the structure along the surface normal is detectable, microbeam grazing incidence small-angle X-ray scattering (μGISAXS) is well suited to investigate structures parallel to the surface, so-called lateral structures and long-ranged correlations. In contrast to AFM, this is not limited to the sample surface, but structures inside the film are probed. Figure 6 shows the line cuts from the two-dimensional μGISAXS data measured for a representative set of nbc-PNIPAM films of different thickness.

In Figure 6a detector scans are shown. The specular peak is blocked with a beam stop to avoid damage to the sensitive detector. In addition to the Yoneda peaks, which are located at the critical angles of the investigated materials (Si and PNIPAM), strong modulations in the intensity are detected. These modulations are caused by a partial phase coherence of X-ray waves diffusely scattered from different interfaces, which yields a concentration of intensity in narrow sheets in reciprocal space. The detector scan cuts through these narrow intensity sheets giving rise to a modulation of the intensity. The necessary condition for observing the partial phase coherence of diffusely scattered waves is a roughness correlation between the SiOx surface and the nbc-PNIPAM surface. Analogous to a thin layer of snow on hills, the thin nbc-PNIPAM film replicates the SiOx surface topography. Thus, a long-ranged correlation between both interfaces is installed and the thickness *d* of the nbc-PNIPAM film determines the distance between adjacent minima

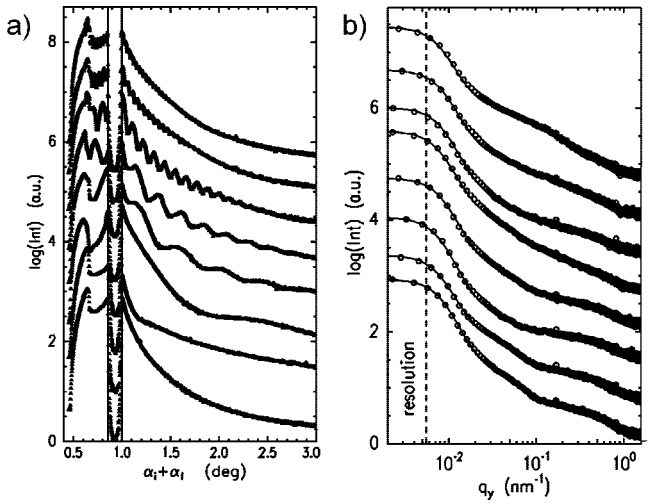

Figure 6. Line cuts from the μGISAXS 2d data for a representative selection of different film thicknesses (5, 7, 8, 22, 35, 74, 154, and 241 nm from bottom to top). (a) Detector scans shown as a function of the detector angle $\alpha_i + \alpha_f$ and (b) out-of plane scans shown as a function of the q_y component of the scattering vector. The solid lines are fits to the data as described in the text. The resolution limit is shown with the dashed line. From bottom to top the film thickness increases and the curves are shifted along the y-axis for clarity.

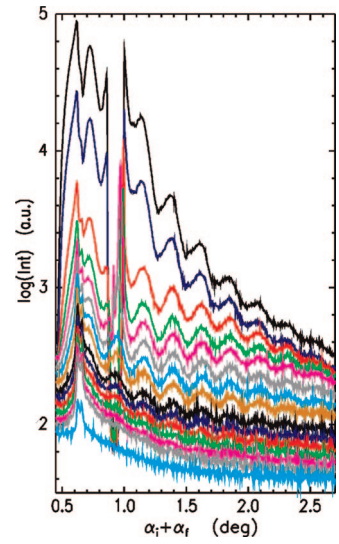

Figure 7. Off-detector scans measured at the angle of incidence $\alpha_i = 0.465°$ for a nbc-PNIPAM film with a film thickness of 35 nm at different values of q_y showing the disappearance of interference fringes of the resonant diffuse scattering. The offset in q_y increases from the top to the bottom. For clarity, the curves are shifted against each other.

in the intensity modulation in the detector scan

$$\Delta q_z = \frac{2\pi}{d} \tag{2}$$

Meanwhile, long-ranged correlation such as roughness replication have been observed in many different types of polymer systems. Most of them were single-layer systems, prepared by spin-coating,[98–101] but multilayer systems and films prepared by other preparation techniques were also reported to show correlated (interface) roughness.[102]

In case of simple homopolymers such as polystyrene, it was shown that the morphology induced during the spin-coating process is dominated by bending elasticity of the freezing polymer solution, resulting in a characteristic cutoff R_c at short wavelengths of the substrate surface roughness spectrum. At the short-wavelength cutoff, a crossover from a conformal to a statistically independent roughness spectrum is observed. For large wavelengths within the limited experimental resolution, the substrate and the polymer−vacuum interface are correlated.[99] For thin hydrogel films so far no experimental evidence of roughness correlation is known to the authors.

Accessing the so-called off-detector scans, the film thickness-dependent increase of the short wavelength cutoff R_c describing the changes in the surface morphology was measured. Figure 7 shows these off-detector scans for a selected film thickness of $d = 35$ nm. From the top to the bottom q_y increases in steps of $\Delta q_y = 1.8 \times 10^{-3}$ nm^{-1}. The curves are shifted against each other for clarity. The amplitude of the fringes resulting from resonant diffuse scattering decreases with increasing q_y. This indicates the loss of correlation at smaller in-plane length scales while at long in-plane length scales the substrate and the polymer−vacuum interface are still correlated. Thus, the behavior of the physically cross-linked thin nbc-PNIPAM hydrogel films is qualitatively identical to the behavior of thin homopolymer films. However, the thickness dependence of the cutoff is different. Within the experimental error, independent of the film thickness a constant cutoff at $R_c = 16.2$ nm is detected. This value is very similar to $2R_H = 15.6$ nm determined for the size of the nbc-PNIPAM objects in dioxane. Thus, one might conclude that the micelle structure installed in solution defines an object size which cannot deform to follow the roughness spectrum of the solid support.

d. Lateral Structures Inside the Dry Hydrogel Films. The adsorption of such micelles or vesicles of polystyrene-*b*-poly(*N*-isopropylacrylamide) (PS-*b*-PNIPAM) diblock copolymers on a gold surface from aqueous solution revealed that the micelles and vesicles were intact with some deformation when they were deposited on the surface.[52] However, on strongly interacting surfaces, the micelles are deformed and even micelle or vesicle fusion into layered films can occur.

nbc-PNIPAM films with thicknesses larger than 5 nm are physically cross-linked hydrogels because during spin-coating with increasing concentration of the deposited nbc-PNIPAM solution on the solid support the bridging of micelles in addition to entanglement favors the gelation. Thus, an internal structure comparable to the microphase separation structure in triblock copolymers with hydrophobic end blocks is expected. Figure 6b shows out-of plane scans cut from the two-dimensional μGISAXS data. None of the scattering curves exhibit a strong intensity peak such as one will expect for microphase-separated systems. Instead, a weak and broad intensity peak at large q_y values is present, and the intensity rises toward smaller q_y values. The rise in intensity is due to the presence of large-scale structures, which are not resolved in the scattering experiment. Such a behavior is very common for many types of polymer thin film systems. Possible origins are contributions of long-ranged surface waves.

Identical to microphase-separated systems, the peak is a structure factor type information, giving a nearest-neighbor distance (e.g., between spheres in a matrix, cylinders in a matrix, or adjacent lamellae in case of a triblock copolymer). Thus, the thin nbc-PNIPAM films exhibit an internal structure, which differs from a well-defined microphase separation. The presence of a weak broad peak, instead of a strong sharp peak, is due to an increased deviation in the nearest-neighbor distances from its mean value, typically expressed with a Gaussian-type distribution with an increased full width at half-maximum. Therefore, in the investigated films the mean distance between adjacent regions of hydrophobic *n*-butyltrithiocarbonate end groups is more broadly distributed than in systems with long end groups. A reason can be the broad distribution of the micellar size in the solution. The out-of plane cuts are fitted

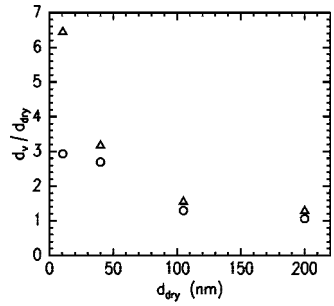

Figure 8. Thickness of the nbc-PNIPAM films exposed to saturated water vapor d_v at 21.7 °C (circles) and 34 °C (triangles) normalized by the thickness of the dry films in air d_{dry}.

with a simplified model. This model accounts for a structure factor due to the distance between neighboring domains of hydrophobic chain ends in the PNIPAM matrix (denoted structure factor 1). Moreover, it includes a structure factor due to the presence of large heterogeneities (denoted structure factor 2) and takes the experimental resolution into account. Both structure factors are distributed with a Gaussian type. The form factor (spherical shape of the micelles) is omitted due to the polydispersity of the micelles as probed in solution and due to the gelation of the micelles in the thin film. The solid lines in figure 6b show the corresponding fits to the out-of plane scans. The resulting mean distance between domains of chain ends is 25 nm. Comparing this value with the micellar size detected in solution shows that the micelles are indeed bridged and entangled inside the film. The resulting distance corresponding to structure factor 2 decreases from 600 to 400 nm with increasing film thickness. In addition, for films with thicknesses lower than 30 nm, structure factor 1 is more pronounced than structure factor 2 while for thicker films, the situation is opposite. Thus, the heterogeneities are more densely populated in thicker films, or in other words, thicker films are less perfect with respect to the inner structure. The nature of the heterogeneities remains undetermined; however, errors in the positioning of hydrophobic domains, such as merging of two or more domains, are quite likely. A possible reason is the increased concentration, which was used in spin-coating film with increased film thicknesses. At high concentrations, already in solution larger, entangled associates of core−shell type micelles might have formed, which embedded in the thin film cause large-scale density inhomogeneities.

4.2. Swelling Experiments. To address the LCST behavior in thin films as a function of the degree of swelling, the films are exposed to saturated water vapor. For this purpose a temperature-controlled swelling chamber with a water reservoir inside was operated. The thickness of dry films and of swollen films is measured as a function of temperature with optical interference. Starting at room temperature, each sample is allowed to equilibrate after each temperature increase by $\Delta T =$ 1 °C for 30 min. Equilibration is concluded from the absence of any changes in the spectra of the optical interference measurements. The reported temperature-dependent changes are reversible. The resulting spectra are fitted including changes in the refractive index due to incorporation of water. The optical constant of PNIPAM is taken as reference for the dry film.

The thicknesses of the dry films agree well with the values determined with X-ray reflectivity. Exposed to saturated water vapor atmosphere, a clear response in terms of swelling is observed at room temperature. Figure 8 shows the very strong film thickness dependence of the total swelling. Ultrathin films with a thickness of 10.5 nm, which is twice the minimum thickness installable for the given surface energy of the SiOx, exhibit a swelling by a factor of 6.5 as compared to the dry film (triangles in Figure 8) and a factor of 2.9 as compared to the collapsed film at 34 °C (circles in Figure 8). With increasing film thickness the nbc-PNIPAM films undergo swelling to a decreasing factor. In case of the 200 nm thick film the swollen film thickness increases only by a factor 1.3 as compared to the dry film. With the net volume change in water for PNIPAM hydrogels being around a factor of 8−10 (changes in volume of a factor of 10 have been reported),[103] corresponding to a one-dimensional size increase of 2−3, the observed swelling factors for ultrathin films are surprisingly high—even more because one needs to take into account that the solid substrate is not deformable and thus a net swelling can only occur in one direction along the surface normal.

In the literature only a few swelling experiments for thin PNIPAM films are performed, and most of them were related to end-grafted PNIPAM.[67–70] The conformation of end-tethered PNIPAM chains with thicknesses below 4 nm and a low surface density at the interface of silicon with D_2O and d-acetone was investigated with neutron reflection. No conformational change with temperature was detected for the lowest molecular weight sample (33K), which is comparable to the PNIPAM block used in this investigation. Only a slight change in conformation with temperature was detected for the higher molecular weight sample (220K).[63] In contrast, for larger film thicknesses of 25−150 nm the swollen film thickness decreased by a factor of 2 upon increasing the temperature from 25 to 40 °C.[104]

For a film thickness range of 5−35 nm Hirata et al.[58] observed a linear increase due to swelling by a factor of 4.6, comparing the dry with the swollen film below the transition temperature. However, the experimental conditions were considerably different because a reactive copolymer (co-PNIPAM) was used, and layers were immobilized on a gold surface with a self-assembled monolayer (OH-SAM) by grafting one chain end to the surface. Moreover, swelling was performed in Dulbecco's phosphate buffered saline without calcium and magnesium (Nissui Pharmaceutical, Tokyo).

Block copolymer films with one PNIPAM block, adsorbed sequentially by the layer-by-layer technique, were observed to show only a very weak response to temperature changes. The decrease in thickness of the adsorbed planar film was below 10% and, moreover, irreversible. The strong interdigitation between adjacent layers in the case of polyelectrolyte multilayers leads to an additional restriction of the chain dynamics and swelling.[105] So one reason for the strong swelling observed in this investigation might be the collapsed chain conformation, which is forced in the dry film due to the applied spin-coating technique. In combination with the hydrophilic substrate surface, which favors the PNIPAM segments as well as water, the swelling might be increased by a type of entropic spring change in the conformation of the micelles. With increasing film thickness this effect gets weaker because fewer nbc-PNIPAM molecules in the micelles are in a perturbed conformation. At a thickness of 40 nm the factor of 3.2 is reached when comparing the dry with the swollen film below the transition temperature. A further increase of the film thickness results in a weaker swelling.

Figure 9 shows the measured LCST behavior. The temperature-dependent changes of the film thickness measured for nbc-PNIPAM films exposed to saturated water vapor decrease with increasing film thickness (see Figure 9a). In the derivative $\delta d/\delta T$ the transition temperature and the width of the transition are visible (see Figure 9b). Within the experimental errors the transition temperature is at 29 °C for the thin films and seems to shift toward lower temperatures for thicker films. In addition, the width of the transition increases with film thickness. The 10.5 nm thick nbc-PNIPAM film exhibits a very sharp transition within a temperature change of 2 °C, which is small as compared

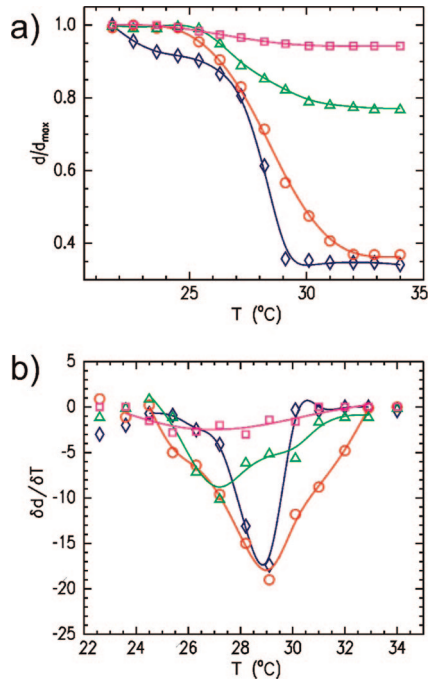

Figure 9. (a) Temperature-dependent changes of the film thickness measured for nbc-PNIPAM films exposed to saturated water vapor and (b) first derivative indicating the transition temperature and the width of the transition. The swelling curves are measured for film thickness of 10.5 (rhombs), 40 (circles), 105 (triangles), and 200 nm (squares). The solid lines are guides to the eye.

to bulk samples, and at 200 nm film thickness the observed transition width is equivalent to the bulk behavior.

The introduction of hydrophobic end groups was observed to decrease the LCST temperature in bulk samples. Thus, in solution we have observed already a decrease of the transition temperature down to 30 °C. In thin films the transition temperature is decreased slightly further, which might result from a confinement into a thin film or from the interaction with the interfaces (substrate and water vapor).

Because of the missing or weak response, which was so far observable in thin films on flat solid supports, confined PNIPAM was realized by encapsulation into polyelectrolyte microcapsules. The transition temperature inside the capsules was observed to be reduced as compared to bulk PNIPAM by 2 °C because the capsule wall protects the PNIPAM, but the transition temperature still follows the trend of a lower LCST with higher salt concentration of the solution.[106]

The missing decrease in the LCST temperature in case of thin plasma polymerized PNIPAM films strongly underlines the sensitivity of the transition to the molecular structure in addition.[53] However, confinement typically would result in a lower transition temperature in stronger confinement, and thus with increasing film thickness the value should approach the bulk value. As a consequence, it is more likely that the interaction with the interfaces affects the transition temperature.

5. Conclusion

Thin nbc-PNIPAM films are successfully prepared on SiOx surfaces using spin-coating. The very short end groups can be regarded as degraded hydrophobic blocks of an ABA-type block copolymer (A denoting a hydrophobic and B a thermosensitive block). The ABA block copolymers can be swollen by midblock selective solvents, leading to the physically cross-linked gels, where the end-block domains form the physical cross-links. This concept still works for very short end groups, and correspondingly our prepared nbc-PNIPAM films exhibit an internal structure due to the microphase separation of the hydrophilic and hydrophobic segments. The structure is expected in the analogy to triblock copolymer films and consists of small spherical domains of hydrophobic chain ends randomly distributed in a matrix of PNIPAM.

In the thin film geometry the thermosensitivity is still present for the investigated nbc-PNIPAm films. Thus, omitting reactive groups, spin-coating results in physically cross-linked hydrogel films on solid supports. These films are not anchored and only attached to the support by the polymer−solid interaction. Therefore, such kind of responsive hydrogel films exhibits a much stronger response to the external stimulus as compared to anchored ones. The transition temperature is only slightly reduced as compared to the bulk. Therefore, the prepared films maintain the interesting features of PNIPAM revealed in the strength of the transition and by the transition temperature which is slightly above room temperature.

Thus, with respect to application, the presented system of end-capped PNIPAM thin films prepared with spin-coating appears to be interesting. In contrast to most other reported thin PNIPAM films, the thickness can be tuned over a wide range (from 5 to 240 nm) and the thermal switching remains possible. This will open novel possibilities in applications ranging from simple switches, solute separation, and drug delivery to tissue culture substrates and controlled adsorption of biopolymers.

Acknowledgment. We thank S. Beuermann (Universität Potsdam) for acces to SEC equipment and A. Timmann for his help during the alignment of BW4 beamline at HASYLAB. We thank W. Doster, TU Munich, for his support during the PCS measurements. Financial support by DFG in the priority program SPP1259 (PA771/4, LA611/7 and MU1487/8) is gratefully acknowledged.

References and Notes

(1) Tanaka, T. *Phys. Rev. Lett.* **1978**, *40*, 820.
(2) (a) Tanaka, T.; Nishio, I.; Sun, S. T.; Ueno-Nishio, S. *Science* **1982**, *218*, 67. (b) *Stimuli-Responsive Water Soluble and Amphiphilic Polymers*; McCormick, C. L., Ed.; ACS Symposium Series 780; The American Chemical Society: Washington, DC, 2001.
(3) Snowden, M.; Murray, M.; Chowdry, B. Z. *Chem. Ind.* **1996**, *14*, 531–534.
(4) Osada, Y.; Kishi, R.; Hasebe, M. *J. Polym. Sci., Part C: Polym. Lett.* **1987**, *25*, 481–485.
(5) Shinohara, S.; Tajima, N.; Yanagisawa, K. *J. Intell. Mater. Syst. Struct.* **1996**, *7*, 254–259.
(6) Osada, Y.; Ross-Murphy, S. B. *Sci. Am.* **1993**, *259*, 42.
(7) Liu, Z.; Calvert, P. *Adv. Mater.* **2000**, *12*, 288–291.
(8) Feil, H.; Bae, Y. H.; Jan, F.; Kim, S. W. *J. Membr. Sci.* **1991**, *64*, 283.
(9) Park, Y. S.; Ito, Y.; Imanishi, Y. *Langmuir* **1998**, *14*, 910.
(10) Rao, K. V. R.; Devi, K. P. *Int. J. Pharm.* **1988**, *48*, 1–13.
(11) Brazel, C. S.; Peppas, N. A. *Polym. Mater. Sci. Eng.* **1996**, *74*, 370–371.
(12) Stayton, P. S.; Shimoboji, T.; Long, C.; Chilkoti, A.; Chen, G.; Harris, J. M.; Hoffman, A. S. *Nature (London)* **1995**, *378*, 472.
(13) Gupta, P.; Vermani, K.; Garg, S. *Drugs Discov. Today* **2002**, *7*, 569–579.
(14) Kikuchi, A.; Okano, T. *Macromol. Symp.* **2004**, *205*, 217–227.
(15) Liang, L.; Rieke, P. C.; Liu, J.; Fryxell, G. E.; Young, J. S.; Engelhard, M. H.; Alford, K. L. *Langmuir* **2000**, *16*, 8016–8023.
(16) Kessler, D.; Theato, P. *Macromol. Symp.* **2007**, *249−250*, 424–430.
(17) Akashi, R.; Tsutsui, H.; Komura, R. *Adv. Mater.* **2002**, *14*, 1808–1811.
(18) Asher, S. A.; Weismann, J. M.; Sunkara, H. B. US Patent 6165389, **2000**.
(19) Mias, S.; Sudor, J.; Camon, H. *Microsyst Technol.* **2007**, Web alert.
(20) Kanazawa, R.; Yoshida, T.; Gotoh, T.; Sakohara, S. *J. Chem. Eng. Jpn.* **2004**, *37*, 59–66.
(21) Miyata, T.; Uragami, T.; Nakamae, K. *Adv. Drug Delivery Rev.* **2002**, *54*, 79–98.
(22) Akiyoshi, K.; Kang, E.-C.; Kurumada, S.; Sunamoto, J.; Principi, T.; Winnik, F. M. *Macromolecules* **2000**, *33*, 3244–3249.
(23) Winnik, F. M. *Macromolecules* **1990**, *23*, 233.

(24) Schild, H. G. *Prog. Polym. Sci.* **1992**, *17*, 163.
(25) Tam, K. C.; Wu, X. Y.; Pelton, R. H. *J. Polym. Sci., Polym. Chem. Ed.* **1993**, *31*, 963.
(26) Tiktopulo, E. I.; Bychkova, V. E.; Ricka, J.; Ptitsyn, O. B. *Macromolecules* **1994**, *27*, 2879.
(27) Wu, C.; Zhou, S. *Macromolecules* **1995**, *28*, 8381.
(28) Wang, X.; Qiu, X.; Wu, C. *Macromolecules* **1998**, *31*, 2972.
(29) Pelton, R. *Adv. Colloid Interface Sci.* **2000**, *85*, 1.
(30) Maeda, Y.; Higuchi, T.; Ikeda, I. *Langmuir* **2001**, *17*, 7535.
(31) Stieger, M.; Richtering, W. *Macromolecules* **2003**, *36*, 8811.
(32) Kita, R.; Wiegand, S. *Macromolecules* **2005**, *38*, 4554.
(33) Lutz, J.-F.; Akfemir, Ö.; Hoth, A. *J. Am. Chem. Soc.* **2006**, *128*, 13046.
(34) Huber, D. L.; Manginell, R. P.; Samara, M. A.; Kim, B. I.; Bunker, B. C. *Science* **2003**, *301*, 352–354.
(35) Matsuyama, A.; Tanaka, F. *J. Chem. Phys.* **1991**, *94*, 781.
(36) Wu, C.; Zhou, S. *Macromolecules* **1995**, *28*, 5388.
(37) Okada, Y.; Tanaka, F. *Macromolecules* **2005**, *38*, 4465.
(38) Taylor, L. D.; Cerankowsky, L. D. *J. Polym. Sci., Polym. Chem. Ed.* **1975**, *13*, 2551.
(39) Kujawa, P.; Winnik, F. M. *Macromolecules* **2001**, *34*, 4130.
(40) Cao, Z.; Liu, W.; Gao, P.; Yao, K.; Li, H.; Wang, G. *Polymer* **2005**, *46*, 5268.
(41) Furyk, S.; Zhang, Y.; Ortiz-Acosta, D.; Cremer, P. S.; Bergbreiter, D. E. *J. Polym. Sci., Part A: Polym. Chem.* **2006**, *44*, 1492–1501.
(42) Kujawa, P.; Segui, F.; Shaban, S.; Diab, C.; Okada, Y.; Tanaka, F.; Winnik, F. M. *Macromolecules* **2006**, *39*, 341–348.
(43) Chung, J. E.; Yokoyama, M.; Suzuki, K.; Aoyagi, T.; Sakurai, Y.; Okano, T. *Colloids Surf. B* **1997**, *9*, 37.
(44) Winnik, F. M.; Davidson, A. R.; Hamer, G. K.; Kitano, H. *Macromolecules* **1992**, *25*, 1876.
(45) Aseyev, V.; Tenhu, H.; Winnik, F. M. In *Self-Organization of Amphiphilic Copolymers in Aqueous Media*; Khokhlov, A. R., Ed.; Springer-Verlag GmbH: Heidelberg, Germany, in press.
(46) Jones, D. M.; Smith, J. R.; Huck, W. T. S.; Alexander, C. *Adv. Mater.* **2002**, *14*, 1130.
(47) Xia, Y.; Qin, D.; Yin, Y. D. *Curr. Opin. Colloid Interface Sci.* **2001**, *6*, 54.
(48) Lenz, P. *Adv. Mater.* **1999**, *11*, 1531.
(49) Kataoka, D. E.; Troian, S. M. *Nature (London)* **1999**, *402*, 794.
(50) Callow, M. E.; Callow, J. A.; Ista, L. K.; Coleman, S. E.; Nolasco, A. C.; Lopez, G. P. *Appl. Environ. Microbiol.* **2000**, *66*, 3249.
(51) Gan, D.; Lyon, L. A. *Macromolecules* **2002**, *35*, 9634.
(52) Yan, Y.; Zhou, X.; Ji, J.; Yan, L.; Zhang, G. *J. Phys. Chem. B* **2006**, *110*, 21055–21059.
(53) Cheng, X.; Canavan, H. E.; Stein, M. J.; Hull, J. R.; Kweskin, S. J.; Wagner, M. S.; Somorjai, G. A.; Castner, D. G.; Ratner, B. D. *Langmuir* **2005**, *21*, 7833–7841.
(54) Tsuji, S.; Kawaguchi, H. *Langmuir* **2005**, *21*, 8439–8442.
(55) Serpe, M. J.; Jones, C. D.; Lyon, L. A. *Langmuir* **2003**, *19*, 8759–8764.
(56) Serpe, M. J.; Lyon, L. A. *Chem. Mater.* **2004**, *16*, 4373–4380.
(57) Mangeney, C.; Ferrage, F.; Jullien, L.; Ouari, O.; Rékaï, E. D.; Laschewsky, A.; Vikholm, I.; Sadowski, J. W. *J. Am. Chem. Soc.* **2002**, *124*, 5811.
(58) Hirata, I.; Okazaki, M.; Iwata, H. *Polymer* **2004**, *45*, 5569–5578.
(59) Nykanen, A.; Nuopponen, M.; Laukkanen, A.; Hirvonen, S.-P.; Rytela, M.; Turunen, O.; Tenhu, H.; Mezzenga, R.; Ikkala, O.; Ruokolainen, J. *Macromolecules* **2007**, *40*, 5827–5834.
(60) You, Y.-Z.; Zhou, Q.-H.; Manickam, D. S.; Wan, L.; Mao, G.-Z.; Oupicky, D. *Macromolecules* **2007**, *40*, 8617–8624.
(61) Iwata, H.; Oodate, M.; Uyama, Y.; Amemiya, H.; Ikada, Y. *J. Membr. Sci.* **1991**, *55*, 119.
(62) Ying, L.; Kang, E. T.; Neoh, K. G.; Kato, K.; Iwata, H. *Macromol. Mater. Eng.* **2003**, *288*, 11–16.
(63) Yim, H.; Kent, M. S.; Huber, D. L.; Satija, S.; Majewski, J.; Smith, G. S. *Macromolecules* **2003**, *36*, 5244–5251.
(64) Yim, H.; Kent, M. S.; Mendez, S.; Lopez, G. P.; Satija, S.; Seo, Y. *Macromolecules* **2006**, *39*, 3420–3426.
(65) Miyamae, T.; Akiyama, H.; Yoshida, M.; Tamaoki, N. *Macromolecules* **2007**, *40*, 4601–4606.
(66) Ishida, N.; Biggs, S. *Macromolecules***2007**, ASAP article.
(67) Yan, Q.; Hoffman, A. S. *Polymer* **1995**, *36*, 887–889.
(68) Kaneko, Y.; Nakamura, S.; Sakai, K.; Aoyagi, T.; Kikuchi, A.; Sakurai, Y.; Okano, T. *Macromolecules* **1998**, *31*, 6099.
(69) Yim, H.; Kent, M. S.; Mendez, S.; Lopez, G. P.; Satija, S.; Seo, Y. *Macromolecules* **2006**, *39*, 3420–3426.
(70) Kaholek, M.; Lee, W.-K.; Ahn, S.-J.; Ma, H.; Caster, K. C.; LaMattina, B.; Zauscher, S. *Chem. Mater.* **2004**, *16*, 3688.
(71) Skrabania, K.; Li, W.; Laschewsky, A. *Macromol. Chem. Phys.,* accepted.
(72) Jakeš, J. *Collect. Czech. Chem. Commun.* **1995**, *60*, 1781.
(73) Müller-Buschbaum, P. *Eur. Phys. J. E* **2003**, *12*, 443.
(74) Braun, C.,1997–99 Parratt32 or The Reflectivity Tool, version 1.5.2 (HMI Berlin).
(75) Roth, S. V.; Döhrmann, R.; Dommach, M.; Kuhlmann, M.; Kröger, I.; Gehrke, R.; Walter, H.; Schroer, C.; Lengeler, B.; Müller-Buschbaum, P. *Rev. Sci. Instrum.* **2006**, *77*, 085106.
(76) Müller-Buschbaum, P.; Bauer, E.; Pfister, S.; Roth, S. V.; Burghammer, M.; Riekel, C.; David, C.; Thiele, U. *Europhys. Lett.* **2006**, *73*, 35.
(77) Yoneda, Y. *Phys. Rev.* **1963**, *131*, 2010.
(78) Salditt, T.; Metzer, T. H.; Peisel, J.; Reinker, B.; Moske, M.; Samwer, K. *Europhys. Lett.* **1995**, *32*, 331.
(79) Müller-Buschbaum, P.; Vanhoorne, P.; Scheumann, V.; Stamm, M. *Europhys. Lett.* **1997**, *40*, 655.
(80) Müller-Buschbaum, P. *Anal. Bioanal. Chem.* **2003**, *376*, 3.
(81) Daillant, J.; Belorgey, O. *J. Chem. Phys.* **1992**, *97*, 5824.
(82) Holy, V.; Baumbach, T. *Phys. Rev. B* **1994**, *49*, 10668.
(83) Xia, Y.; Burke, N. A. D.; Stover, H. D. H. *Macromolecules* **2006**, *39*, 2275–2283.
(84) Zhou, X.; Ye, X.; Zhang, G. *J. Phys. Chem. B* **2007**, *111*, 5111.
(85) Garret-Flaudy, F.; Freitag, R. *J. Polym. Sci., Part A* **2000**, *38*, 4218.
(86) Lin, S.-Y.; Chen, K.-S.; Chu, L.-R. *Polymer* **1999**, *40*, 2619.
(87) Percot, A.; Zhu, X. X.; Lafleur, M. *J. Polym. Sci., Polym. Phys.* **2000**, *38*, 907.
(88) Katsumoto, Y.; Tanaka, T.; Sato, H.; Ozaki, Y. *J. Phys. Chem. A* **2002**, *106*, 3429.
(89) Schild, H. G. *Prog. Polym. Sci.* **1992**, *17*, 163.
(90) Hirokawa, Y.; Tanaka, T.; Matsuo, E. S. *J. Chem. Phys.* **1984**, *81*, 6379.
(91) Zhou, S.; Wu, C. *Macromolecules* **1996**, *29*, 4998–5001.
(92) Müller-Buschbaum, P.; Maurer, E.; Bauer, E.; Cubitt, R. *Langmuir* **2006**, *22*, 9295.
(93) Walter, H.; Harrats, C.; Müller-Buschbaum, P.; Jérôme, R.; Stamm, M. *Langmuir* **1999**, *15*, 1260.
(94) Mahltig, B.; Müller-Buschbaum, P.; Wolkenhauer, M.; Wunnicke, O.; Wiegand, S.; Gohy, J. F.; Jerome, R.; Stamm, M. *J. Colloid Interface Sci.* **2001**, *242*, 36.
(95) Lawrence, C. J. *Phys. Fluids* **1988**, *31*, 2786.
(96) Spangler, L. L.; Torkelson, M.; Royal, J. S. *Polym. Eng. Sci.* **1990**, *30*, 644.
(97) Schubert, D. W. *Polym. Bull.* **1997**, *38*, 177.
(98) Müller-Buschbaum, P.; Stamm, M. *Macromolecules* **1998**, *31*, 3686.
(99) Müller-Buschbaum, P.; Gutmann, J. S.; Lorenz, C.; Schmitt, T.; Stamm, M. *Macromolecules* **1998**, *31*, 9265.
(100) Müller-Buschbaum, P.; Gutmann, J. S.; Kraus, J.; Walter, H.; Stamm, M. *Macromolecules* **2000**, *33*, 569.
(101) Müller-Buschbaum, P.; Gutmann, J. S.; Lorenz-Haas, C.; Mahltig, B.; Stamm, M.; Petry, W. *Macromolecules* **2001**, *34*, 7463.
(102) Kraus, J.; Müller-Buschbaum, P.; Stamm, M.; Bucknall, D. *J. Polym. Sci., Phys.* **1999**, *37*, 2862.
(103) Hirotsu, S.; Yamamoto, I.; Matsuo, A.; Okajim, T.; Furukawa, H.; Yamamoto, T. *J. Phys. Soc. Jpn.* **1995**, *64*, 2898.
(104) Otsu, T.; Matsumoto, A. *Adv. Polym. Sci.* **1998**, *136*, 75.
(105) Steitz, R.; Leiner, V.; Tauer, K.; Khrenov, V.; v. Klitzing, R. *Appl. Phys. A* **2002**, *74*, S519−S521.
(106) Prevot, M.; Déjugnat, C.; Möhwald, H.; Sukhorukov, G. B. *ChemPhysChem* **2006**, *7*, 2497–2502.

MA7027775